-Electronic Supplementary Information (ESI)-

Crystalline/amorphous nickel sulfide interface for high current density in alkaline HER: Surface and Volume confinement matters!

Prince JJ Sagayaraj, and Karthikeyan Sekar*

Sustainable Energy and Environmental Research Laboratory, Department of Chemistry, Faculty of Engineering and Technology, SRM Institute of Science and Technology, Kattankulathur, Chennai 603203, Tamil Nadu, India.

Corresponding author Karthikeyan Sekar*

E-mail: karthiks13@srmist.edu.in

Experimental section

Chemicals

Nickel (Ni) foam 99.9% 1.6 mm thickness (MTI Korea), Thiourea, (SRL), Potassium hydroxide (Thermo Fisher Scientific Ltd.), Ammonium chloride (NH_4Cl), Nickel II chloride hexahydrate, ethanol 99.9% (Changshu Song Sheng Fine Chemicals) were purchased and used as such. Distilled water with 18.2 MΩ from NANO pure Diamond UV deionized water purification system was used for all the synthesis and studies.

Synthesis method

Dynamic Hydrogen Bubble Template method for depositing Porous Ni on Ni foam (NN)

Ni foam is cut into 1cm × 2cm dimensions and pretreated with 1.5M HCl to remove oxidised surface and further washed with acetone and ethanol to remove any impurities. Ni foam is connected against Ag/AgCl reference electrode (RE) and Pt wire (counter electrode (CE)) in a solution containing 0.1M $NiCl_2$ and 2M NH_4Cl. A constant potential of -1.3V vs. Ag/AgCl is applied for 600 s under hydrogen evolution region. Then, the Ni deposited Ni foam (NN) is taken out washed with distilled water and ethanol and dried in vacuum oven for few hours.

Hydrothermal synthesis of Ni_3S_2 on NN (NNS)

The NN electrode is sealed in 50 mL Teflon lined stainless steel autoclave containing 1:1 mole ratio of CSN_2H_4 and KOH respectively, kept in hot air oven at 120°C for 24hr. The autoclave is allowed to cool naturally and the resultant foam (NNS) seemed to change its colour

indicating the successful sulphurisation process. The NNS is washed several times with distilled water to remove any impurities and then followed by ethanol, then dried in vacuum.

Electrodeposition of Ni_xS_y on NNS (NNS/NNS_x)

The electrodeposition process was carried out with suitable modification adapting the previous literature.[1] Briefly, NNS/NNS_x is synthesized using NNS as WE by potentiostatic deposition for 600 s (-1.8V vs. Ag/AgCl, Pt wire as CE) in an electrolytic solution containing 50 mL of 1:1:10 mole ratio of $NiCl_2$, NH_4Cl and CSN_2H_4 respectively. The black foam is taken out washed with water and ethanol several times and dried in vacuum. NNS_x is synthesised by same process using bare NF as WE.

Characterisation

Physical Characterisation

To confirm the crystalline phase X-ray Diffraction analysis (XRD) was done using Malvern PANanalytical equipped with Empyrean Cu X-ray tube with K_α radiation and Pixel3D detector running at 0.02° step scan rate. The topography and morphology of the material were asserted using Field Emission Scanning Electron Microscopy (FE-SEM), Thermoscientific Apreo S and elemental mapping EDS with FEI QUANTA accelerating with 0.02 MV. Hi-resolution Transmission Electron Microscopy (HR-TEM) images was taken using JEOL Japan, JEM-2100 Plus to study the atom arrangements, defects and interplanar distances. Surface compositions and the chemical states of the catalysts were assessed using X-ray Photoelectron spectroscopy (XPS) PHI Versaprobe III. The HORIBA, LabRam HR Evolution MicroRaman Spectrometer was used to indicate the presence of chemical bonds in the material.

Electrochemical characterisation

The whole experiment is carried out in 1.0M KOH, pH 14 being set-up in a conventional three electrode cell model, using Hg/HgO as RE and Ni foam as CE for HER. The electrochemical workstation CHI760E screened the electrochemical studies at room temperature. (Geographical location 12.8250223, 80.0439124).

HER studies: The developed electrocatalysts were activated electrochemically by cyclic voltammetry (CV) for several cycles at a scanrate of 50 mVs^{-1} against Open Circuit Potential (OCP) to ensure optimum hydrogen saturation around the working electrode (WE). Linear Sweep Voltammetry (LSV) was done at the lowest scanrate 1 mVs^{-1} with 100% *iR* compensation. Electrochemical Impedance Spectroscopy (EIS) is operated under catalytic turn-over conditions with AC amplitude 5mV in the wide frequency range 0.1 Hz - 100MHz form which Nyquist, Bode-absolute impedance and Bode phase angle measurements are calculated to interpret charge-transfer rate. Sampled Current Voltammetry (SCV) studies were adapted as mentioned in the previous literature[2] to avoid expendable charging current from LSV. Double layer capacitance (C_{dl}) method is adapted by increasing the scan from 10 to 200 mVs-1 for CV in the non-Faradaic region to study charge-discharge phenomenon. Electrochemically accessible sites (ECAS) are calculated by integrating the charge under Ni^{3+} to Ni^{2+} reduction curve as in the earlier studies.[3] The long-term stability of the material is tested by amperometry studies. All the data obtained from CHI760E is plotted and the graphs are obtained using Microsoft excel.

Firstly, 100% *iR* compensations were made and then converted into universal scale of RHE using the following equation.

$$E_{RHE} = E_{Hg/HgO} + E^{\circ}{}_{Hg/HgO} + \frac{2.303\,RT}{F}pH \qquad \text{(S1)}$$

$E^{\circ}{}_{Hg/HgO}$ – calibrated everytime using standard method of carrying out HER with Pt foil

R – universal gas constant (8.314 $JK^{-1}mol^{-1}$)

T – room temperature in °C

F – Faraday constant (96485 C mol^{-1})

Tafel analysis was done in the HER region was calculated from the following Tafel equation,

$$\eta = a - b \log j \qquad \text{(S2)}$$

where "η" is the overpotential E - E_{iR} vs. RHE in V, "a" is Tafel constant, "b" is Tafel slope in V dec^{-1} and "j" is current density in mA cm^{-2}.

The Tafel constant "a" was calculated by the following equations:

$$\textbf{Intercept, a} = \frac{2.303\ RT}{\alpha nF}\ \textbf{log}\ j_0 \tag{S3}$$

$$\alpha n = \frac{2.303\ RT}{bF} \tag{S4}$$

Here "α" is the transfer coefficient, "j_0" is the exchange current density in mA cm^{-2}

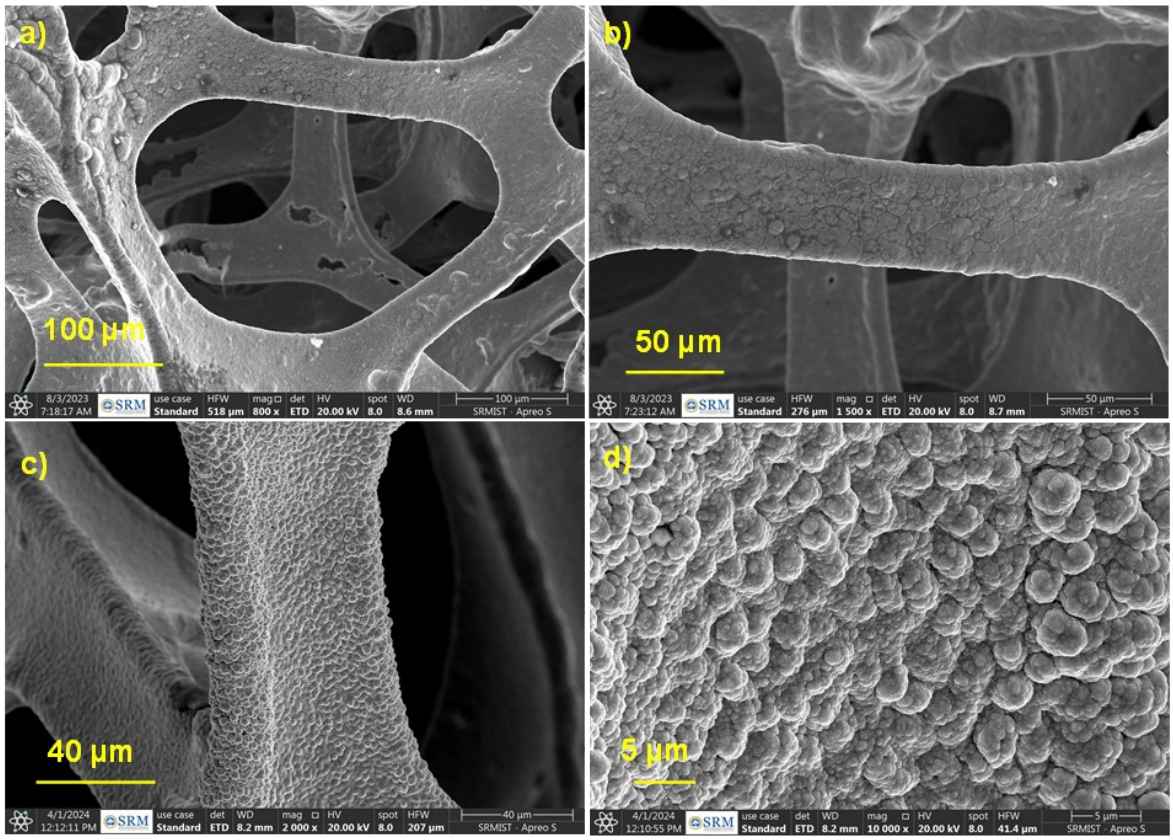

Fig.S1 (a-d) FE-SEM images of NN showing porosity under different magnifications.

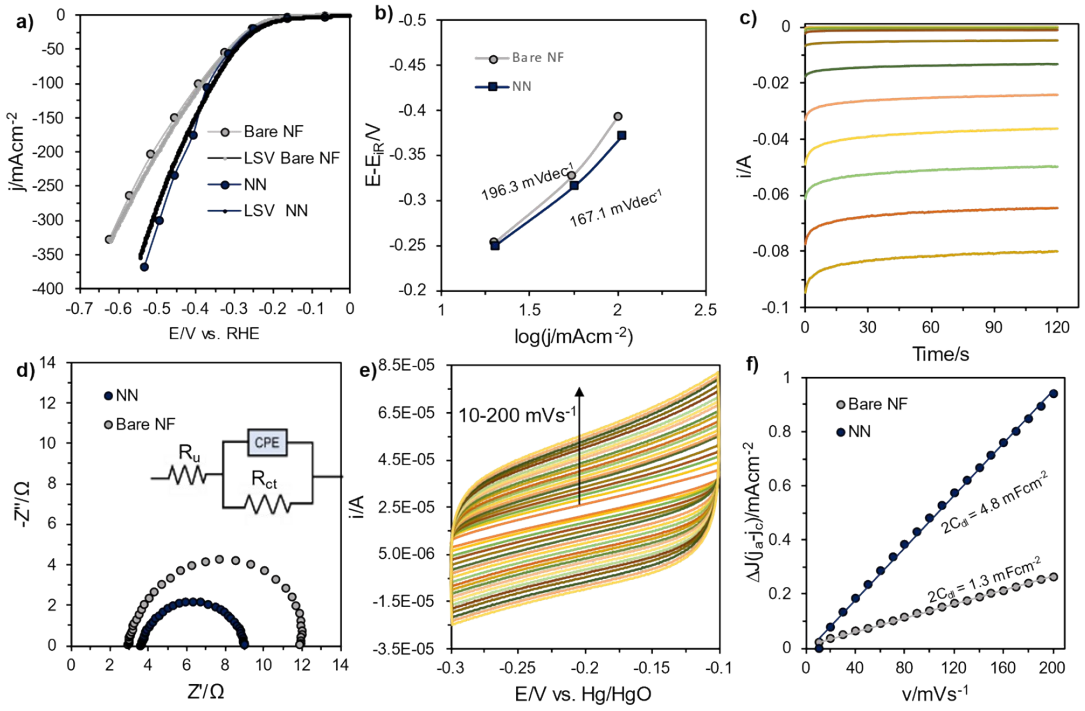

Fig.S2 (a) LSV and SCV plots, (b) Tafel plots extracted from SCV for bare NF and NN respectively, (c) CA responses of bare NF at a constant potential of -0.8V to -1.8V at 100 mV interval vs.Hg/HgO for 120s, (d) Nyquist plot (inset shows equivalent circuit), (e) CV responses in the Non-Faradaic region from the scanrate 10 mV^{s-1} to 200 mVs^{-1} of bare NF and (f) Linear plot of double-layer charging current density versus scan rate for bare NF and NN.

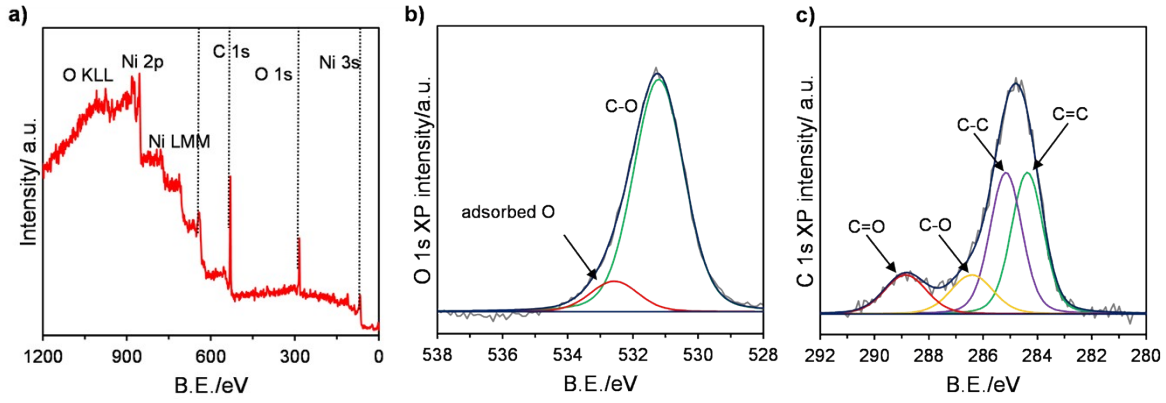

Fig. S3 (a) XPS survey spectra, Core level (b) O1s and (c) C1s spectra for NNS/NNS$_x$.

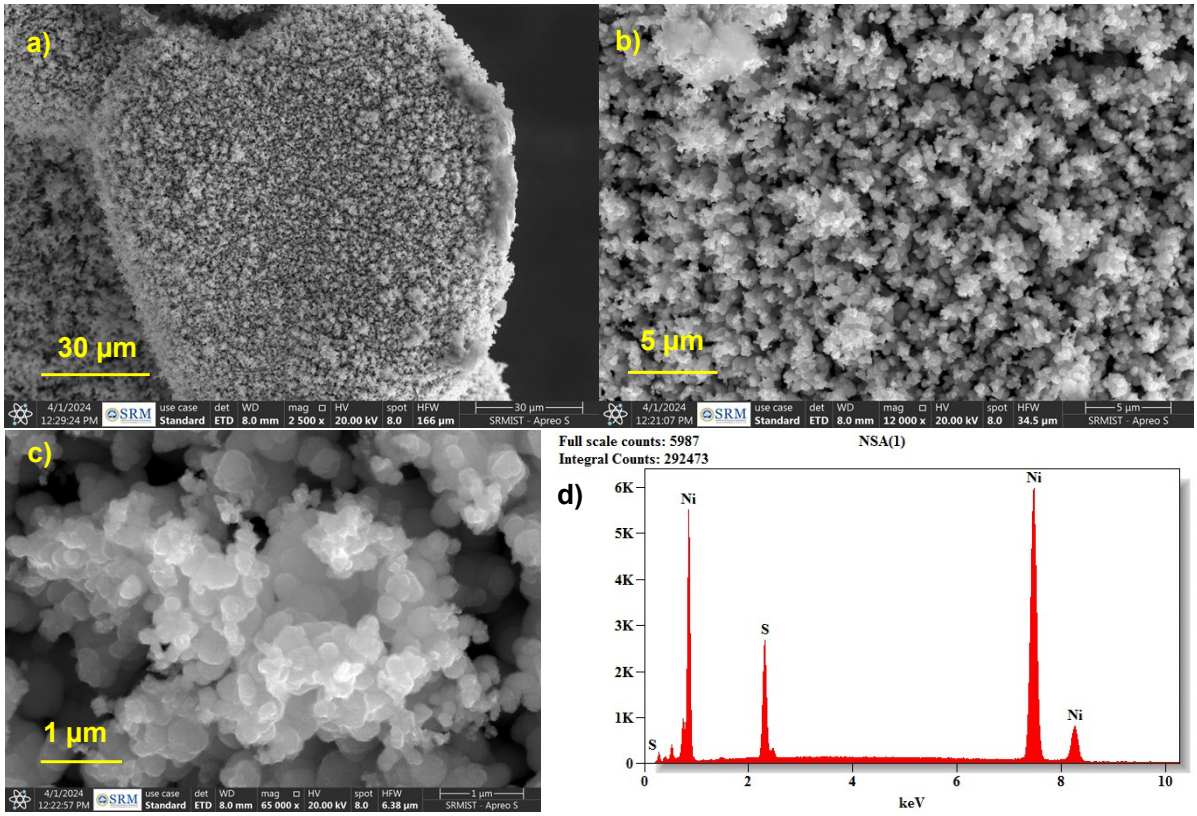

Fig. S4 (a-c) FESEM images under different magnification and (d) EDX spectra of NNS/NNS_x.

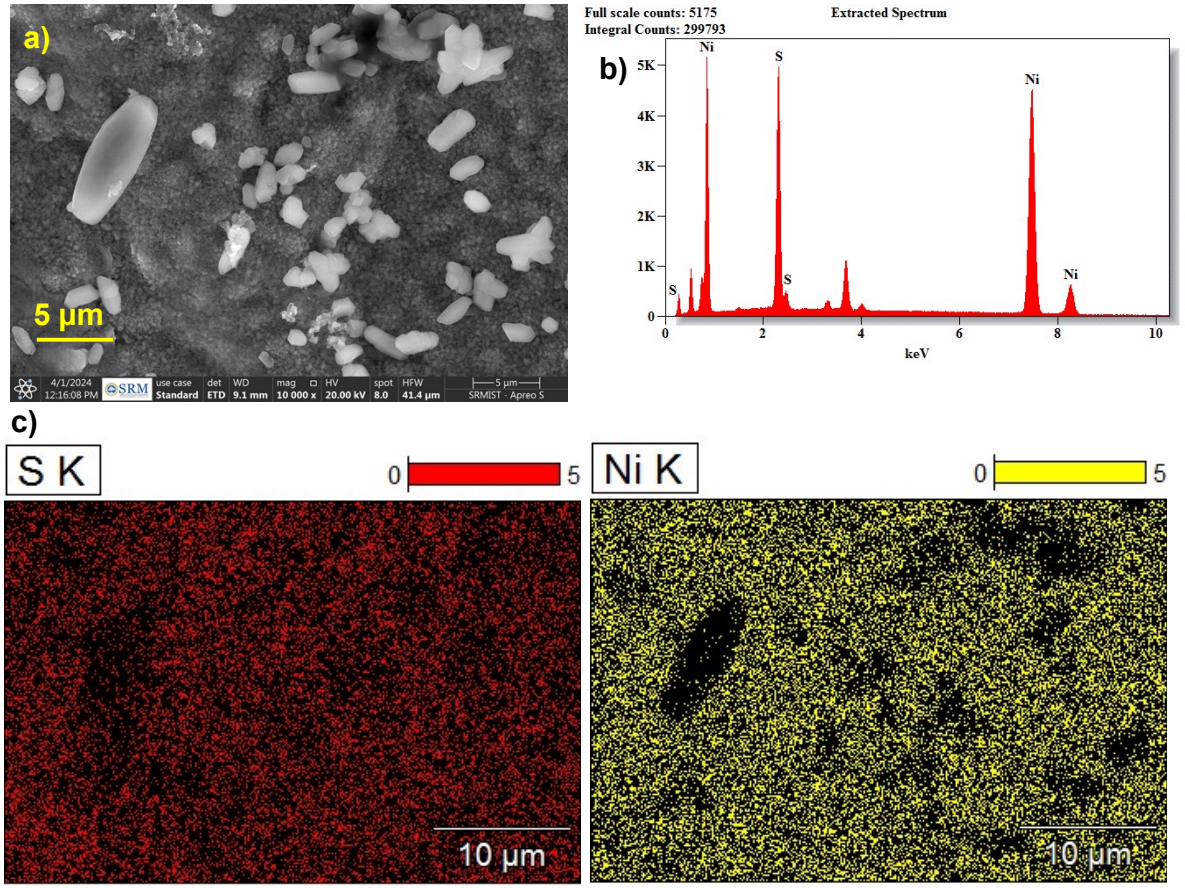

Fig. S5 (a) FESEM image, (b) EDX spectra and (c) Elemental mapping for the elements Ni and S of NNS.

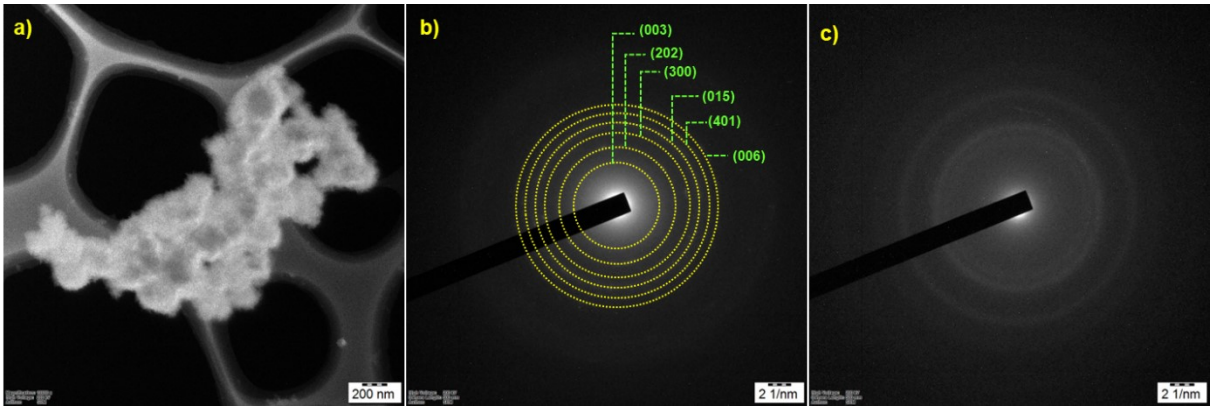

Fig. S6 (a) Dark Field Scanning Transmission Microscopic (STEM) image, (b) and (c) SAED pattern of NNS/NNS$_x$.

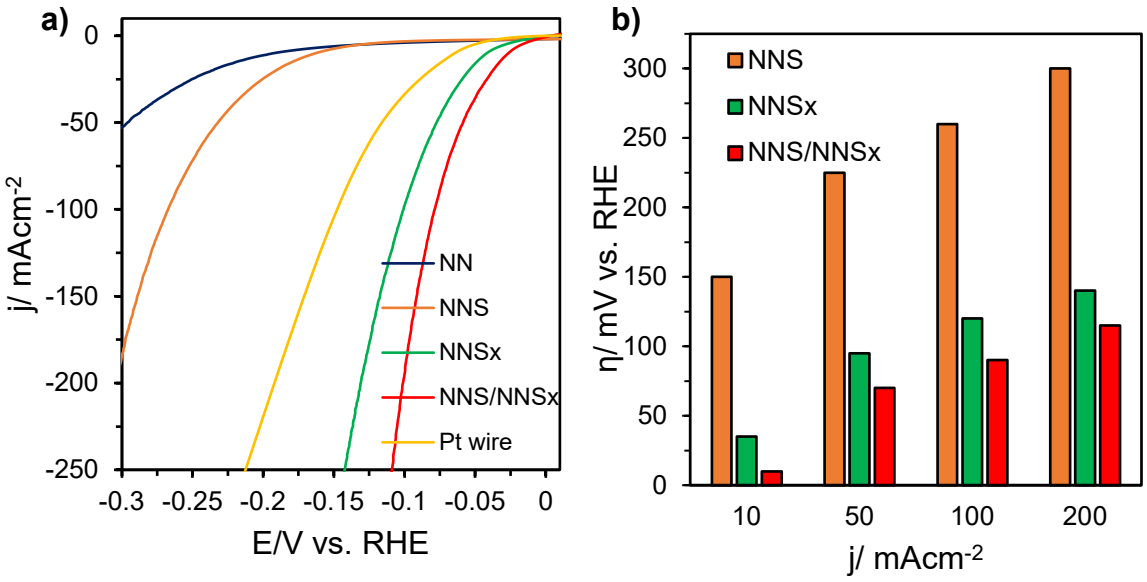

Fig.S7 (a) LSV plot recorded at a scan-rate of 1 mVs^{-1} in 1.0 M KOH with 100% *iR* compensation and (b) Comparative plots of overpotential at 10, 50, 100 and 200 $mAcm^{-2}$ current density for different electrocatalysts.

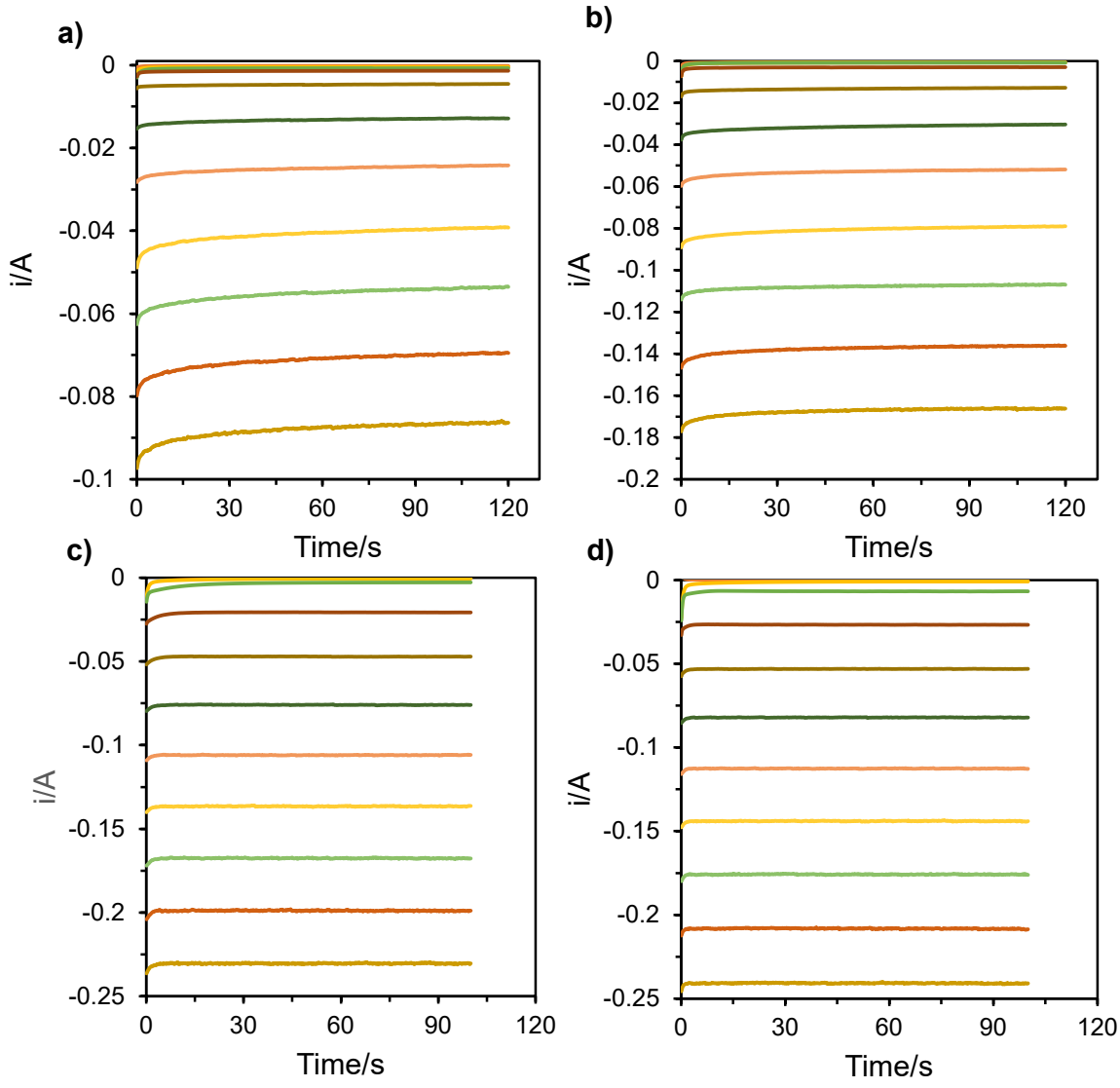

Fig. S8 CA responses at a constant potential of -0.8V to -1.8V at 100 mV interval vs.Hg/HgO for 120s of (a) NN, (b) NNS, (c) NNS_x, and (d) NNS/NNS_x respectively.

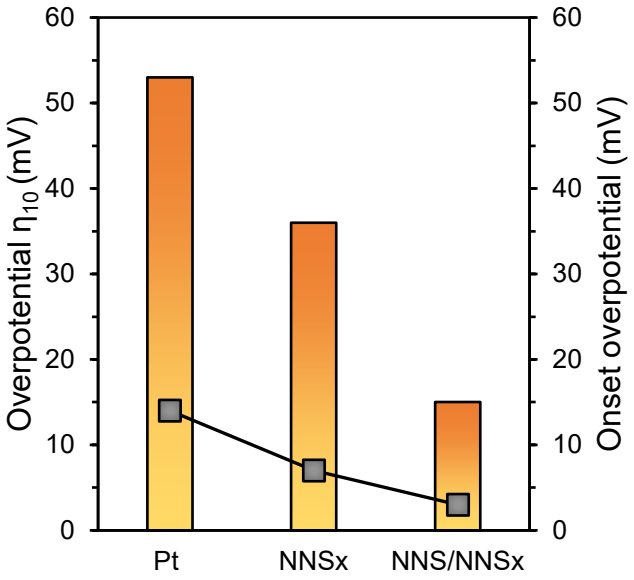

Fig. S9 Plot showing overpotential at 10 $mAcm^{-2}$ and their respective onset overpotential for HER of Pt, NNS_x and NNS/NNS_x

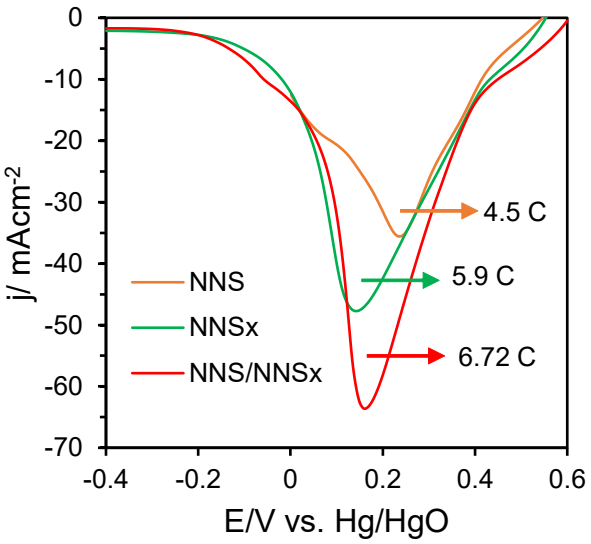

Fig. S10 The backward sweeps of CVs 1.0 M KOH used for calculating ECAS

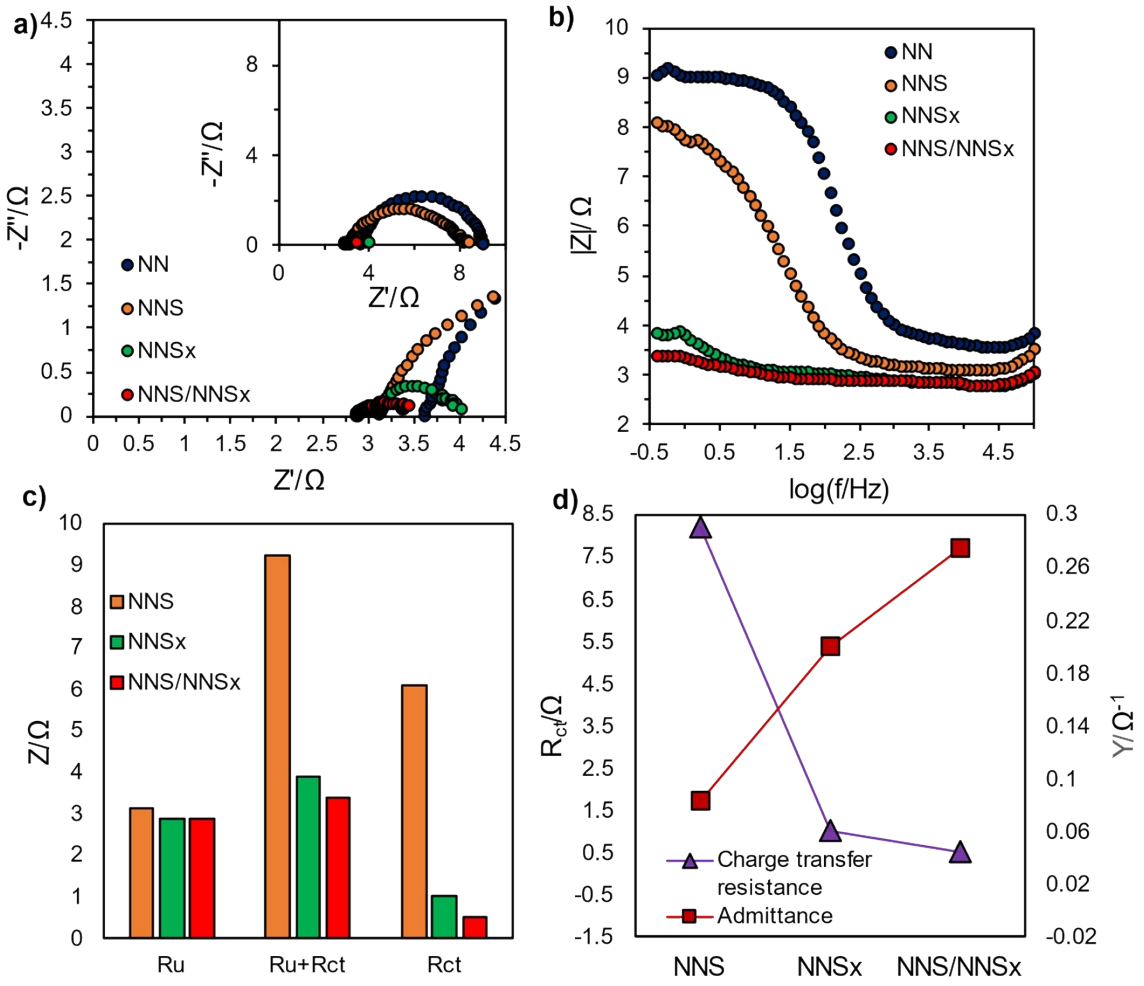

Fig. S11 (a) Nyquist plot (Inset showing complete semi-circle), (b) Bode-absolute impedance recorded at -1.2V vs. Hg/HgO at 5mV amplitude with an operating frequency between 0.1Hz and 100MHz, (c) Bar chart comparatively showing uncompensated and charge-transfer resistances and (d) Comparative line graph of resistance and admittance for NNS, NNS_x, and NNS/NNS_x respectively.

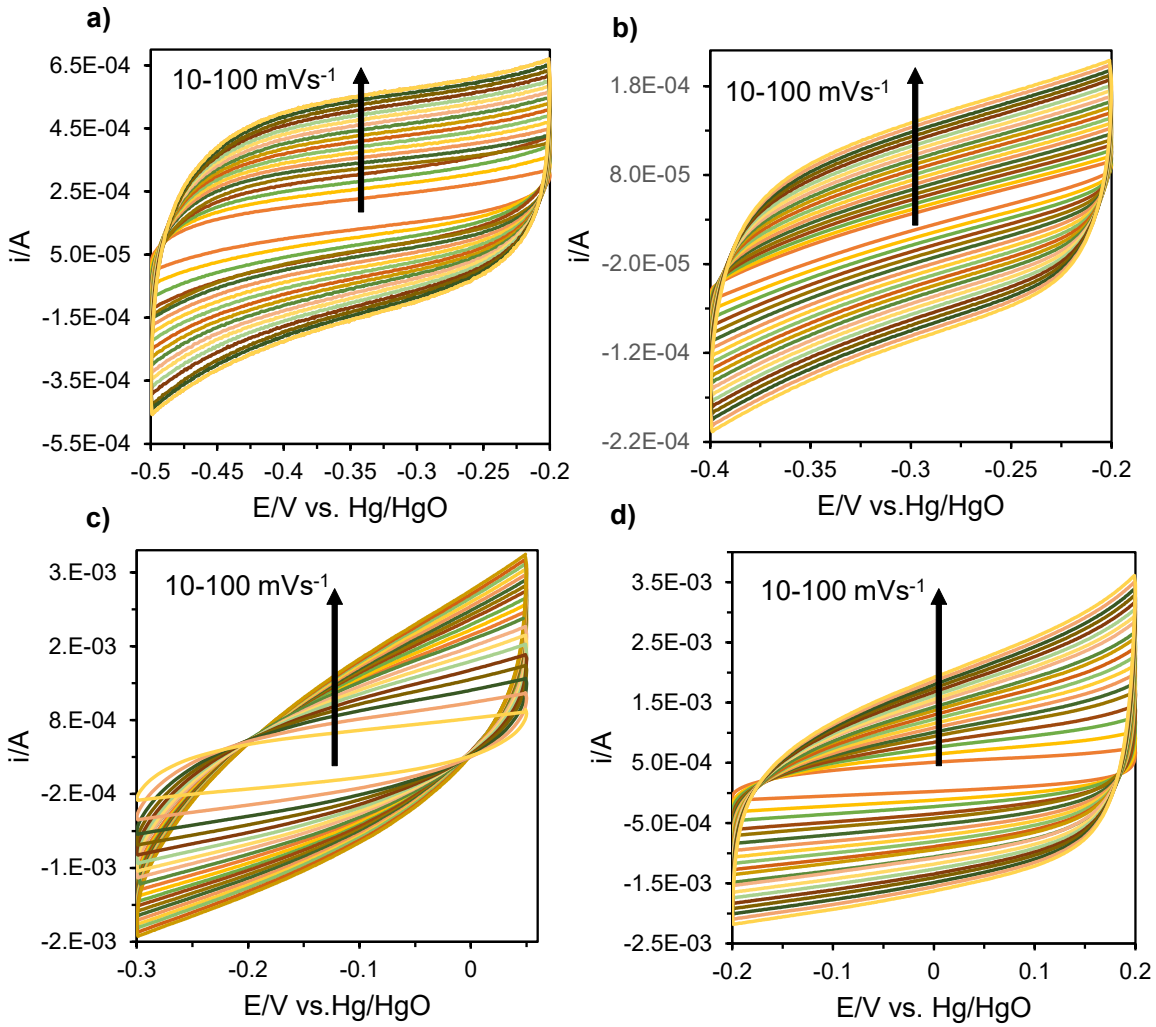

Fig. S12 CV responses in the non-Faradaic region for calculate C_{dl} values of (a) NN, (b) NNS, (c) NNS_x and (d) NNS/NNS_x respectively.

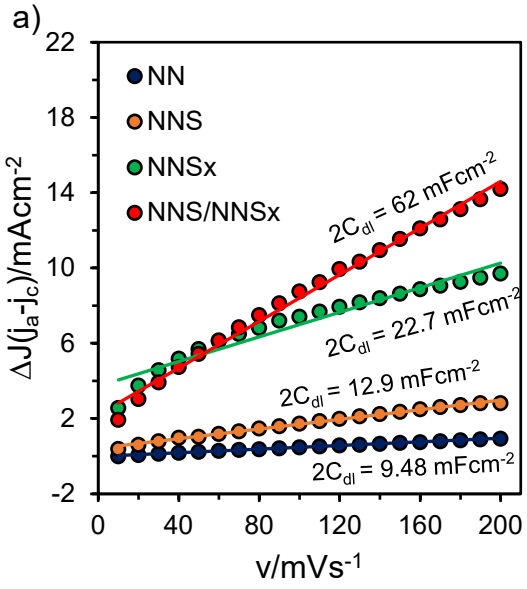

Fig. S13 Plot of double-layer charging current density recorded in the non-Fardaic region versus scan rate for NN, NNS, NNS_x and NNS/NNS_x.

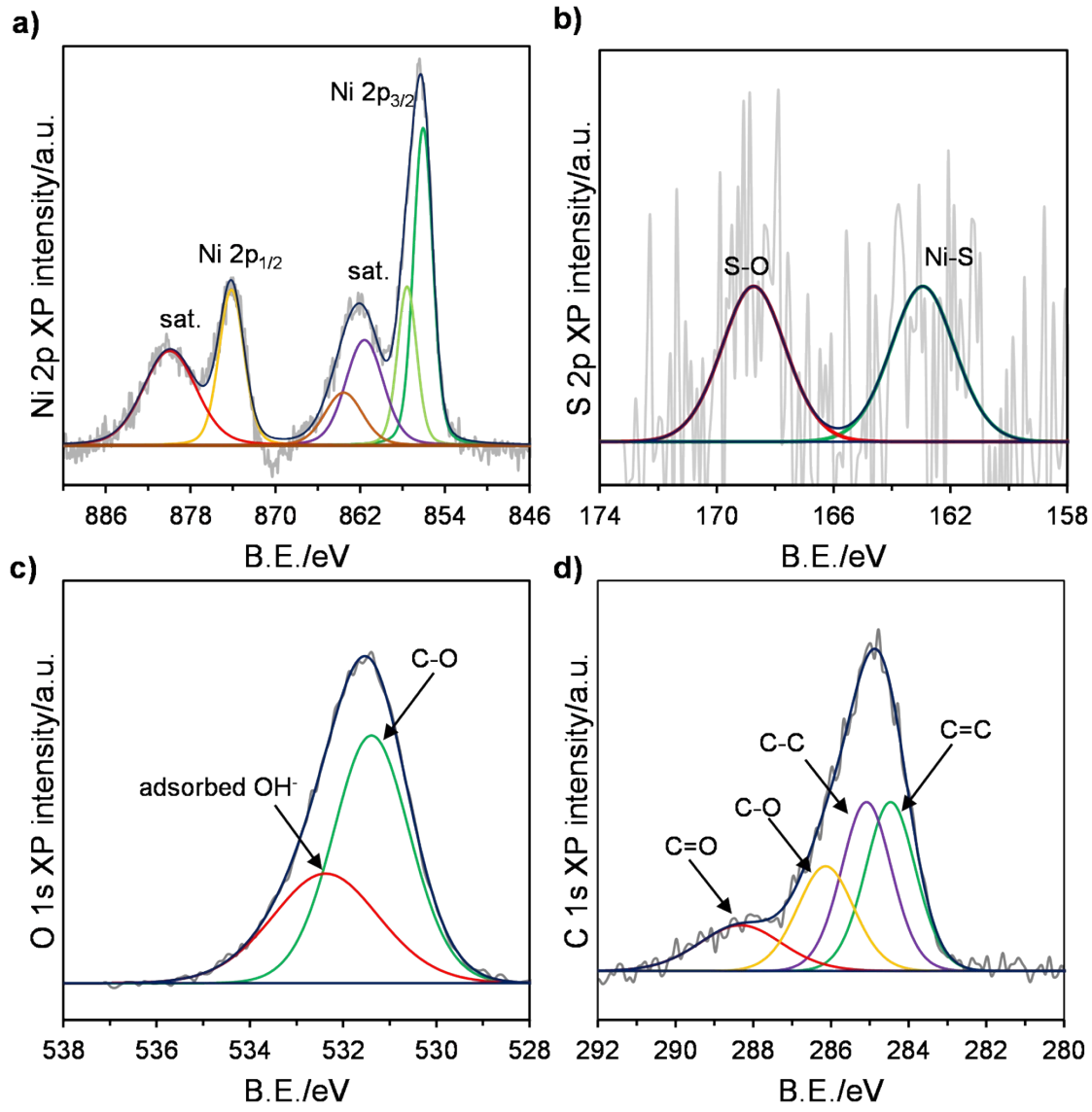

Fig. S14 Core level (a) Ni2p, (b) S2p, (c) O1s and (d) C1s spectra for NNS/NNS$_x$ after HER accelerated degradation results.

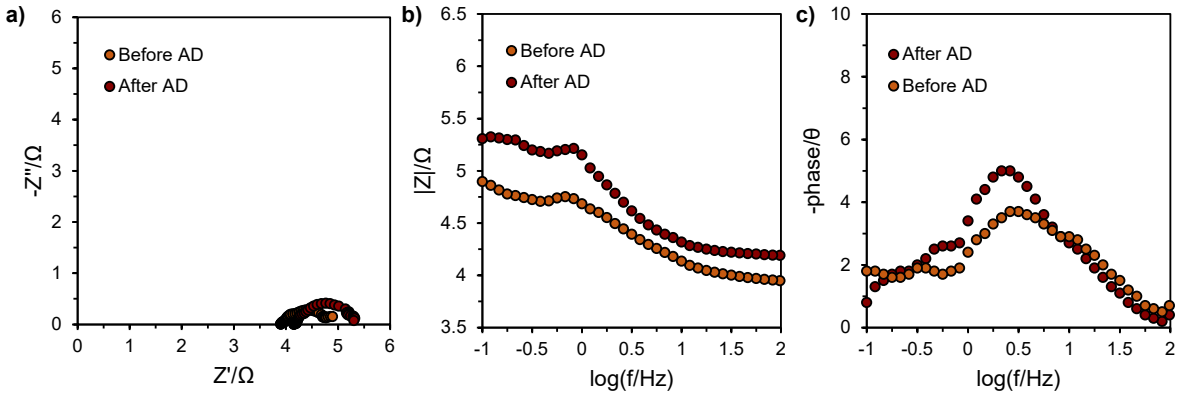

Fig. S15 EIS results (a) Nyquist plot, (b) Bode-absolute impedance plot and (c) Bode-phase angle plot for NNS/NNS$_x$ showing before and after HER accelerated degradation.

Table S1. Comparison table for the electrochemical activity of alkaline hydrogen evolution reaction with various electrocatalysts

Electrocatalyst	**Overpotential, η_{10} (mV)**	**Maximum j ($mAcm^{-2}$) and η_j (mV)**	**Tafel slope (mV dec^{-1})**	**Onset overpotential (mV)**	**Reference**
NiS nanoflower	97	100 and 280	65.90	600	4
Ni_3S_2@CNTs/CC	381	120 and 550	-	250	5
α-NiS@NDCDs/NF	173	-	81	117	6
DLHCs@Ni_xS_y	263	-	88.23	162	7
Vs-Ni_3S_2/NF)	88	100 and 218	87	50	8
Amorphous $Ni_{3.09}S$	43.8	120 and 150	79.9	-	9
Pt_3Ni_2 NWs-S/C	42	35 and 70	-	10	10
Ni_xS/NF	113	80 and 320	90	25	11
O−Ni_3S_2	68.4	800 and 290	60.62	100	12
Ni_3S_2/Ni_xS_y	**15**	**1200 and 180**	**68.5**	**3**	**This work**

1. B. Zhong, S. Wan, P. Kuang, B. Cheng, L. Yu and J. Yu, *Applied Catalysis B: Environmental*, 2024, **340**, 123195.
2. S. Anantharaj, S. Kundu and S. Noda, *Journal of the Electrochemical Society*, 2022, **169**, 014508.
3. S. Anantharaj, P. E. Karthik and S. Noda, *Journal of Colloid and Interface Science*, 2023, **634**, 169-175.
4. B. Zhang, X. Li and M. Liu, *International Journal of Electrochemical Science*, 2024, 100579.
5. R. C. Gotame, Y. R. Poudel, B. Dahal, A. Thapa, C. Dares and W. Li, *International Journal of Hydrogen Energy*, 2024, **51**, 671-680.
6. C. Pitchai, S. M. Gopalakrishnan and C.-M. Chen, *Energy & Fuels*, 2024.
7. C. Liu, X. Zhang, Y. Cheng, X. Hao and P. Yang, *Electrochimica Acta*, 2024, **477**, 143751.
8. D. Jia, L. Han, Y. Li, W. He, C. Liu, J. Zhang, C. Chen, H. Liu and H. L. Xin, *Journal of Materials Chemistry A*, 2020, **8**, 18207-18214.
9. C. Miao, X. Zheng, J. Sun, H. Wang, J. Qiao, N. Han, S. Wang, W. Gao, X. Liu and Z.-x. Yang, *ACS Applied Energy Materials*, 2021, **4**, 927-933.
10. P. Wang, X. Zhang, J. Zhang, S. Wan, S. Guo, G. Lu, J. Yao and X. Huang, *Nature communications*, 2017, **8**, 14580.
11. Z. Fang, Y. Wang, Y. Zou, Z. Hao and Q. Dong, *Inorganic Chemistry Communications*, 2017, **79**, 1-4.
12. X. Zheng, L. Zhang, J. Huang, L. Peng, M. Deng, L. Li, J. Li, H. Chen and Z. Wei, *The Journal of Physical Chemistry C*, 2020, **124**, 24223-24231.